Radiation Physics and Chemistry 79 (2010) 1111–1114

Contents lists available at ScienceDirect

Radiation Physics and Chemistry

journal homepage: www.elsevier.com/locate/radphyschem

Characterisation of individual pixel efficiency in the PILATUS II sensor

A. Schubert [a,c,d,*], G.J. O'Keefe [d,a], B.A. Sobott [a,c], N.M. Kirby [b], R.P. Rassool [a,c]

[a] School of Physics, University of Melbourne, Parkville, 3010, Australia
[b] Australian Synchrotron, Clayton, Victoria 3168, Australia
[c] CRCBID Cooperative Research Centre for Biomedical Imaging, Bundoora, Victoria 3083, Australia
[d] Centre for PET, Austin Hospital, Heidelberg, Victoria 3084, Australia

ARTICLE INFO

Article history:
Received 21 April 2010
Accepted 21 June 2010

Keywords:
Detector efficiency
Charge collection efficiency
Pixel detectors
PILATUS
TCAD
3D modelling

ABSTRACT

Synchrotron applications such as protein crystallography and small-angle X-ray scattering (SAXS) demand precise knowledge of detector pixel efficiency for data corrections. Current techniques used to determine detector efficiency are only applicable for the specific set-up for which the calibration is performed. Here the effect of comparator thresholding on pixel efficiency for PILATUS is presented for standard amplifier and shaper gain settings, allowing users to make necessary corrections to their intensity data for various threshold settings without requiring repeated empirical calibrations. A three-dimensional TCAD simulation of the sensor is also presented and is used to confirm the experimental result.

1. Introduction

State-of-the-art hybrid pixel detectors (HPDs) such as PILATUS (Broennimann et al., 2006) possess superior imaging properties when compared to other detector technologies such as very large dynamic range, very low noise, high local and global count rates, high quantum efficiency, short read-out time and small point spread function. These properties lead to the wide-spread use of HPDs in applications such as SAXS (Basil et al., 2010), protein crystallography (Broennimann et al., 2004; Huelsen et al., 2006) and medical imaging (Moy, 2000).

In a typical HPD, charge generated in the sensor by an impinging photon is converted to a voltage pulse and then amplified and shaped before passing to a discriminator which outputs a digital pulse if a predetermined threshold is exceeded by the incoming charge. The discriminator is followed by a scalar, which allows fully digital storage and readout of the number of detected photons per pixel.

A potential drawback of HPDs is that X-rays impinging on the sensor at a pixel boundary may lead to double counting of a hit due to diffusion of charge, or the hit may be lost to recombination processes. To avoid double counting the comparator threshold value, E_{th}, is set to $E_{th\ 0}=0.5E_0$, where E_0 is the maximum photon energy. If the threshold is set lower than $E_{th\ 0}$ some X-rays converting close to the pixel boundaries are counted in adjacent pixels. A higher threshold than $0.5E_0$ may be required for fluorescence suppression, however, this leads to a reduced count rate as in some cases the partial charge on a pixel does not exceed the threshold.

Many applications require knowledge of detector pixel efficiency for data correction. For example, in SAXS measurements it is used to calculate absolute scattering intensities (Zhang et al., 2009). The scattering intensity $I_s(Q)$ of a sample is proportional to: the incident beam intensity I_0; the scattering differential cross-section per unit volume of the sample $I(Q)$; the sample exposure area A (usually the beam size); sample thickness; sample transmission T; the detector view angle for accepting photons $\Delta\Omega$ (detector slit opening) and the detector efficiency e such that

$$I_s(Q) = I_0 I(Q) A t T \Delta\Omega e \quad (1)$$

Measuring $I_s(Q)$ of an unknown sample is typically conducted by calibrating the instrument using a sample of well known absolute $I(Q)$, which yields an empirical instrument factor $f(=I_0 A\Delta\Omega e)$ valid under fixed measurement conditions. However, there are many other reasons why it can also be useful to understand the detector efficiency, such as optimizing detector efficiency for different experiments, comparing the performance of various detectors, or for measuring absolute scattering intensity directly rather than relying on reference samples. There are numerous factors which affect the sensitivity of silicon-based photon-counting detectors. Perhaps the most obvious would be transparency losses due to finite sensor thickness, which is dependent only on material properties and is therefore a constant

* Corresponding author at: School of Physics, University of Melbourne, Parkville, Australia 3010. Tel.: +61 03 8344 5451.
E-mail address: aschub@physics.unimelb.edu.au (A. Schubert).

0969-806X/$ - see front matter © 2010 Elsevier Ltd. All rights reserved.
doi:10.1016/j.radphyschem.2010.06.008

for any specific sensor. The focus of this paper is the effect of comparator thresholding on pixel efficiency for PILATUS, for standard amplifier and shaper gain settings. This allows users to make necessary corrections to their intensity data for various threshold settings without requiring repeated empirical calibration.

2. The sensor

Discussions of semiconductor physics as it applies to silicon sensors may be found in many publications, for example Lutz (1999), Rossi et al. (2006) and Sze and Ng (2007). Only a brief discussion of the most relevant physics is included here.

In the PILATUS II HPD, pixels are formed via pn-junctions consisting of 112 μm square p+ implantations at 172 μm pitch. These are placed into a highly resistive (approx 8 $k\Omega$ cm) n-type silicon bulk. The sensor is reverse-biased by the application of 120 V voltage to fully deplete the sensor. Full depletion may be estimated from

$$V_{dep} = \frac{eN_D d^2}{2\varepsilon_0 \varepsilon_{Si}} \tag{2}$$

where N_D is the substrate doping (Rossi et al., 2006). Signal charge liberated by a photon via the photoelectric effect is collected by the electric field and is measured at the electrode. The number of generated electron–hole pairs, N_{eh}, is proportional to the energy of the incoming photon, E_p, with $N_{eh} \simeq E_p/3.6$ eV, where 3.6 eV is the average energy required to liberate one electron–hole pair in silicon. In the case of a highly segmented sensor with the read-out electronics mounted on the p-side of the sensor, the majority of the signal is induced by the holes as they near the collection electrode. For holes with a mobility of $\mu_p = 505\,\mathrm{cm^2\,V^{-1}\,s^{-1}}$ a sensor thickness d of 320 μm and a bias voltage V_b of 120 V a drift time of

$$t_d = d^2/(\mu_p V_b) \simeq 15\,\mathrm{ns} \tag{3}$$

is expected. As the charges drift, the charge cloud broadens due to diffusion. The Gaussian distribution for a charge cloud generated at the back of the sensor is given by

$$\sigma_x = [(kT/q)\mu_p t_d]^{1/2} \simeq 6.7\,\mu\mathrm{m} \tag{4}$$

where $kT/q = 0.026$ at 300 K (Lutz, 1999). This demonstrates that photons absorbed at pixel boundaries may thus create a signal in more than one pixel and in the worst case in four pixels at the same time. In such a case the detector measures a lower charge, subsequently leading to either over or under counting depending on the comparator threshold.

3. Experiment

Monitoring the current magnitude over time for individual pixels enables a detailed study of charge sharing behaviour within the sensor. To simulate the charge injection of a 10 keV X-ray a 904 nm laser diode is focussed on the sensor via an optical fibre and a lens. A section of the aluminium layer on the sensor back is etched to allow transmission of optical wavelengths. The etching acid comprises; phosphoric acid 73.0%, nitric acid 3.1%, acetic acid 3.3% and water 20.6%.

Using this set-up, the charge collection efficiency (CCE) profile of individual pixels can then be measured by raster scanning the laser across a single pixel. For this purpose the laser focussing optics are mounted on a micro-precision xy-stage and moved relative to the sensor in 10 μm steps in both x and y. The contour map formed by such a two-dimensional scan is shown in Fig. 1.

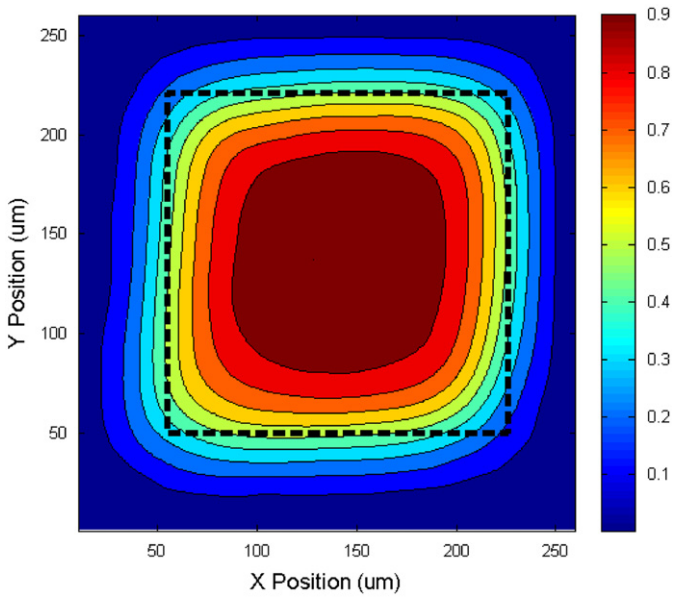

Fig. 1. The experimentally measured collection efficiency profile of a standard design pixel. The dotted line indicates the pixel boundary and is overlaid for reference.

Laser output stability is monitored by returning to a reference location before every scan in the x-direction. This allows the data to be corrected for changes in the laser behaviour over time.

The applicability of infra-red lasers to silicon sensor characterisation has been demonstrated many times, for example Shaheen et al. (1995). However, the method has limitations which must be considered. These are only briefly reviewed here and are discussed in more detail in Krizmanic et al. (1996). The Gaussian width of the laser profile leads to much greater spread than the point-like interaction of a 10 keV X-ray (Lutz, 1999). Additionally, the chosen laser wavelength of 904 nm results in an absorption length of 37 μm leading to all charge being generated near the surface of the sensor. Consequently, the degree of charge spread is then overestimated leading to an underestimation of pixel efficiency at thresholds above $E_{th\,0}$. Laser measurements therefore provide a lower bound on the pixel efficiency in the normal operating regime.

Linear scans over partially etched pixels, where the aluminium extended into the linear-response region of the pixel, yielded an estimate of the spatial profile of the laser in terms of the spatial deviation, $\sigma = (18.8 \pm 2)\,\mu\mathrm{m}$.

The effective area (EA), the pixel area which registers hits for a given energy threshold, can then be calculated from the CCE profile, it is quoted as a fraction of the total pixel area (TA) which is equal to $172 \times 172\,\mu\mathrm{m}$. This provides a measure of the relative pixel efficiency for the detector at different energy thresholds.

4. Simulation

For validation of the experimental results a simulation of the sensor is performed using the ISE-TCAD suite of programs (ISE-TCAD, 2003) in a finite-element method (FEM) approach. Sensor geometry is initialised using the module MESH. This results in a user-defined discretisation of the sensor by forming nodal points (or mesh) at which the physical properties of the detector are specified. Equations specific to the simulation are then solved at these nodal points, providing an initialisation of the sensor. Realistic limitations preclude the implementation of a sub-micron spacing of nodal points, or mesh, and so to ensure numerical